PROTEINS
STRUCTURE ■ FUNCTION ■ BIOINFORMATICS

Mechanistic studies of the apical sodium-dependent bile acid transporter

Raphael Alhadeff, Assaf Ganoth,* and Isaiah T. Arkin

Department of Biological Chemistry, The Alexander Silberman Institute of Life Sciences, The Hebrew University of Jerusalem, Edmond J. Safra Campus Givat Ram, Jerusalem, 91904, Israel

ABSTRACT

In mammals, the apical sodium-dependent bile acid transporter (ASBT) is responsible for the reuptake of bile acid from the intestine, thus recycling bile acid that is secreted from the gallbladder, for the purpose of digestion. As bile acid is synthesized from cholesterol, ASBT inhibition could have important implications in regulation of cholesterol levels in the blood. We report on a simulation study of the recently resolved structures of the inward-facing ASBT from *Neisseria meningitidis* and from *Yersinia frederiksenii*, as well as of an ASBT variant from *Yersinia frederiksenii* suggested to be in the outward-facing conformation. Classical and steered atomistic simulations and comprehensive potential of mean force analyses of ASBT, both in the absence and presence of ions and substrate, allow us to characterize and gain structural insights into the Na^+ binding sites and propose a mechanistic model for the transport cycle. In particular, we investigate structural features of the ion translocation pathway, and suggest a third putative Na^+ binding site. Our study sheds light on the structure–function relationship of bacterial ASBT and may promote a deeper understanding of transport mechanism altogether.

Proteins 2015; 00:000–000.

Key words: membrane protein; molecular dynamics; Na^+-binding; transport mechanism.

INTRODUCTION

Bile acids are synthesized from cholesterol in the liver, secreted into the bile, and stored in the gallbladder. During the digestion process, the gallbladder contracts, and, consequently, bile acids are squeezed into the small intestine, where they facilitate absorption of fatty acids, cholesterol, and water-insoluble vitamins. More than 90% of the bile acids are reabsorbed from the intestine and transported back to the liver via the portal-venous circulation.[1] In humans, this recycling process is mediated by two Na^+-dependent bile acid transporters, one of which is the apical sodium-dependent bile acid transporter (ASBT, a.k.a. SLC10A2).[2] The SLC10A gene family consists of seven Na^+-dependent bile acid transporter members that play important roles not only in enterohepatic circulation of bile acids but also in transporting other solutes, including drugs and viruses (for comprehensive recent reviews see Refs. 3 and 4).

From a pharmaceutical perspective, ASBT is a potential pharmacological target for hypercholesterolemia because ~50% of cholesterol is eliminated from the body by its conversion into bile acids. Accordingly, specific inhibitors of ASBT were found to lower plasma cholesterol levels in animal models.[5,6] ASBT is up-regulated in diabetic mice, and its inhibition by a potent inhibitor lowered glucose levels in an animal model of Type 2 diabetes. This inhibitor is currently tested at clinical trials in patients with Type 2 diabetes.[7] ASBT may also be a medicinal target for some types of inflammatory bowel disease, in particular in Crohn's disease and ulcerative colitis where it was shown to be down-regulated.[8]

However, although the potential medical implications of ASBT inhibitors are promising, usage of ASBT inhibitors is associated with an increased risk for gallstone

Additional Supporting Information may be found in the online version of this article.

Grant sponsor: The Rudin Fellowship Trust (to R.A.); Grant sponsor: The Lady Davis Fellowship Trust to (A.G.); Grant sponsor: The Valazzi-Pikovsky Fellowship Fund (to A.G.); Grant sponsor: Israeli Science Foundation (to I.T.A); Grant number: 1581/08.

*Correspondence to: Assaf Ganoth, The Interdisciplinary Center (IDC), Herzliya 46150, Israel and The Department of Biology and Environment, The Faculty of Natural Sciences, University of Haifa-Oranim, Tivon 36006, Israel.
E-mail: assaf.ganoth@mail.huji.ac.il

Received 14 November 2014; Revised 25 February 2015; Accepted 9 March 2015
Published online 26 March 2015 in Wiley Online Library (wileyonlinelibrary.com). DOI: 10.1002/prot.24796

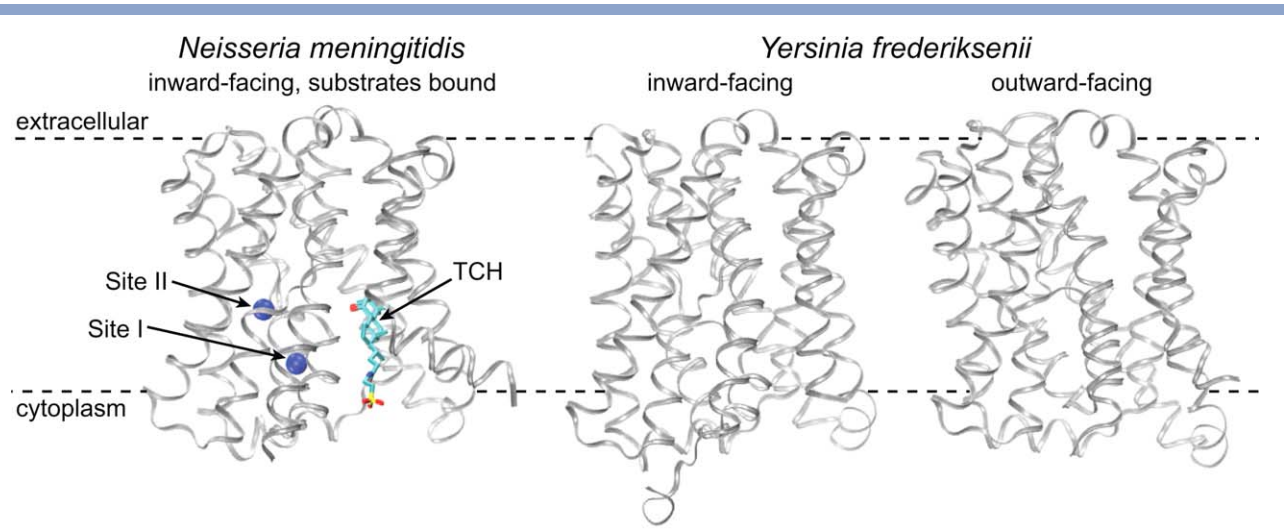

Figure 1

The solved structures of ASBT, shown in a ribbon representation.[20,21] Sodium ions appear as blue spheres. The taurocholate molecule appears in a licorice representation. [Color figure can be viewed in the online issue, which is available at wileyonlinelibrary.com.]

disease,[9] bile acid-induced diarrhea,[10] and cancer.[11,12] Molecular computational models for FDA-approved ASBT inhibitors were constructed,[13] whereas the diverse roles taken by bile acids in colon and gastrointestinal cancers were recently detailed in Ref. 14. Therefore, although the importance of ASBT as a therapeutic target is high, the adverse physiological applications of its inhibition should be carefully monitored and evaluated.

ASBT is a symporter, exploiting the Na^+ gradient to translocate bile acids across the membrane, with a stoichiometry of two Na^+ ions for one bile acid molecule.[15] Biochemical characterization of the human ASBT included extensive mutation screening analyses, which revealed disruption of the protein's stability,[16] interference of the protein's substrate translocation,[17] and triggering of primary bile acid malabsorption, leading to an idiopathic diarrhea.[18] Analysis of the SLC10A2 gene identified a variety of sequence variants, including coding region single nucleotide polymorphisms that influence bile acid intestinal function and homeostasis.[19]

Recently, the crystal structure of a bacterial homologue of ASBT from *Neisseria meningitidis* (NmASBT) was determined in an inward-facing conformation, and at the presence of the substrate taurocholate (TCH) and two Na^+ ions (PDB: 3ZUY).[20] Subsequently, two additional crystal structures of ASBT, from *Yersinia frederiksenii* (YfASBT), were solved in an inward-facing conformation (PDB: 4N7W), and as an E254A mutant that was suggested to be in an outward-facing conformation (PDB: 4N7X).[21] The three ASBT structures, presented in Figure 1, exhibit similar topology; the protein has cytoplasmic amino and carboxy termini, contains 10 transmembrane (TM) helices, and possesses two additional helices that are relatively parallel to the cytoplasmic side of the membrane. The TM helices form two inverted repeat units, each made of a V-shaped motif (TM1 and TM2; TM6 and TM7) and a core motif (TM3–TM5; TM8–TM10). TM1–TM5 and TM6–TM10 are structurally homologous but oppositely orientated, thus producing an internal twofold pseudosymmetry. TM4 and TM9 are discontinuous and crossover at a conserved region, and a wide crevice, to which a substrate is bound, is found at the intracellular side of the protein. Discontinuous TM helices can be found at numerous secondary active transporters, including the Na^+/H^+ antiporter NhaA, the leucine transporter LeuT, and the H^+/Cl^- exchanger ClC.[22] The overall general fold architecture of both NmASBT and YfASBT is highly similar to that of NhaA, although they do not share discernible sequence homology.[23]

Two models were suggested, so far, for the transport mechanism of ASBT: a simplified transport mechanism comprising only the inward-facing structure of NmASBT and a model structure of its outward-facing conformation[20]; and an elaborate transport model, based upon the NmASBT, both YfASBT structures, and three hypothetical conformations.[21] According to the elaborated model, a large rigid-body rotation of the substrate binding domain of the protein, which is located where TM4 and TM9 transverse, accounts for the alternating accessibility mechanism. However, the suggested structural changes of the protein were only hypothetical because they were inferred from two solved inward-facing conformations, one presumably outward-facing conformation, and speculative intermediate conformations. This hampers the ability to track conformational dynamic changes of the protein and to follow the movement of the Na^+ ions along the transport mechanism stages, and calls for an in-depth study that can expand the structural information with computational methods.

Table I
Summary of the simulations performed for the NmASBT and YfASBT

Type	TCH	NaI	NaII	NaIII	Note
MD	−	−	−	−	Only NmASBT
MD	−	+	−	−	NmASBT and IF-YfASBT
MD	−	+	+	−	NmASBT and IF-YfASBT
MD	−	−	+	−	All structures
MD	−	−	+	+	Only OF-YfASBT
MD	−	−	−	+	Only OF-YfASBT
MD	+	−	−	−	All structures
MD	+	+	−	−	NmASBT and IF-YfASBT
MD	+	+	+	−	NmASBT and IF-YfASBT
MD	+	−	+	−	All structures
MD	+	−	+	+	Only OF-YfASBT
MD	+	−	−	+	Only OF-YfASBT
SMD	−				All structures, force on Na^+
SMD	+				All structures, force on Na^+
PMF	−				All structures, Na^+ sampled
PMF	+				All structures, Na^+ sampled
PMF		−	−	−	Only NmASBT, TCH sampled
PMF		+	−	−	Only NmASBT, TCH sampled
PMF		−	+	−	Only NmASBT, TCH sampled
PMF		−	−	+	Only NmASBT, TCH sampled

Each MD simulation was 100 ns long. Total simulation time was ∼ 4 μs.
IF, inward-facing conformation; OF, outward-facing conformation.

By performing classical molecular dynamics (MD) simulations, steered MD (SMD) simulations, and potential of mean force (PMF) calculations and analyses, we present dynamic mechanistic structural insights into the transport mechanism of ASBT. Besides expanding the structural information and proposing intermediate states that were not accessible by the X-ray structures, we uncover a third ion binding site that is proposed to be occluded at specific states of the transport cycle. Finally, based on the X-ray structures and our computational results, we suggest a model for the transport cycle that takes into account the conformational dynamics of the protein and the third ion binding site.

METHODS

Systems setup

In each system, summarized in Table I, a monomeric protein with its crystallographic water molecules was inserted into a pre-equilibrated 1-palmitoyl-2-oleoyl-sn-glycero-3-phosphoethanolamine (POPE) bilayer.[24] The systems' total charge was neutralized by adding Na^+ and Cl^- ions to a final concentration of 137 mM. The systems were subjected to energy minimization using the steepest descent algorithm with a tolerance of 1000 kJ mol^{-1} nm^{-1}, followed by a step using the conjugated gradient algorithm with a tolerance of 100 kJ mol^{-1} nm^{-1}. Three equilibration steps of 100 ps each, under positional restraints using harmonic force constants of $k = 1000$, 500, and 0 kJ mol^{-1} nm^{-2} respectively, were conducted. The equilibrated systems were subjected to 100 ns of unbiased MD production runs.

MD details

All simulations were done using version 4.5.5 of the GROMACS package,[25,26] employing an extended version of the GROMOS53a6 force field[27]; using the LINCS algorithm,[28] allowing a time step of 2 fs; using the Nosé–Hoover temperature coupling at 310 K; employing a semi-isotropic Parrinello–Rahman pressure coupling at 1 bar, differentiating the *z*-axis (the membrane normal); using a cutoff of 1.2 nm for van der Waals interactions; and computing long-range electrostatic interactions with the PME algorithm.[29]

Parameters for the TCH molecule were obtained using the Automated Topology Builder version 2.0,[30] with slight modifications based on similarity to known molecules already existing in the GROMACS database. The TCH molecule was then submitted to an MD simulation in water for equilibration and parameters validation. The position of the TCH in the YfASBT structures were based on docking performed using PatchDock.[31]

Positions for the sodium ions and TCH in the YfASBT inward-facing structure were based on the NmASBT crystal structure.[20] In the outward-facing structure, sodium ions were placed in Sites II and III based on the NmASBT simulations (see Results section), and the TCH orientation was selected based on the arguments presented by Zhou *et al.*[21]

His-tags were removed *in silico* from the structures, and charged termini were used. Furthermore, in the outward-facing structure, the mutated E254A was reverted *in silico* to Glu.

Steered MD

Prior to conduction of the umbrella sampling calculations, SMD simulations were performed to generate a series of consecutive configurations along the chosen reaction coordinate,[32] the *z*-axis which represents the membrane normal. Some of these configurations served as the starting configurations for the PMF calculations, which were run in independent umbrella sampling window simulations. For that end, we performed two SMD simulations, with and without TCH, where a sodium ion was placed in Site II and pulled along the *z*-axis, in each direction, using a moving harmonic force applied to the sodium ion at 500 kJ mol^{-1} nm^{-2}, moving at 0.02 pm ps^{-1} (or at 0.025 pm ps^{-1}), having the protein's center-of-mass as the reference group. Further description for our choice of these force and speed conditions is provided in the Supporting Information.

To ensure that we use enough configurations along the reaction coordinate, in order to obtain reasonable spacing of the umbrella sampling windows, in terms of distance between the ion and the center-of-mass of the protein, we initially chose ∼27 *z*-positions (windows),

separated by $\Delta z \sim 0.1$ nm. These windows cover the studied range of the membrane width, and the bulk water on both sides of the bilayer. Upon completion, we looked at the corresponding histograms (see Supporting Information Fig. S1) and submitted several additional conformations. This process was repeated until the corresponding histogram curves expressed sampling that was complete and thorough, meaning no unsampled regions along the *z*-axis were detected. The iterative process resulted in different numbers of configurations for each condition (for example, the numbers of windows on Supporting Information Fig. S1 are 56 and 33 for the ion and the TCH, respectively).

Potential of mean force

PMF curves were produced using the umbrella sampling method,[33] with sufficient frames for complete sampling of the reaction coordinate and convergence of the PMF. For each starting configuration for the calculation of the PMF, which was obtained from a snapshot of the SMD simulations, the system was independently subjected to an energy minimization to allow the ion to move laterally in the *x-y* plane. The minimization was performed for each window using the steepest descent algorithm and a tolerance of 1000 kJ mol^{-1} nm^{-1}, followed by a minimization using the conjugated gradient algorithm with a sequential decreasing convergence from 100 to 10 kJ mol^{-1} nm^{-1}. Subsequently, a 10 ns production run was performed for each window to collect sampling data. Unbiasing and integration were performed with 200 bins and a tolerance of 10^6 using the weighted histogram analysis method (WHAM).[34] Additional technical methodological information, including histograms of the vertical distribution within the umbrella sampling and error bars, is given in the Supporting Information (Supporting Information Figs. S1 and S2, respectively).

Visualization and analysis

The simulations were visualized with the visual MD (VMD) program.[35] The analyses were conducted using in-house VMD Tcl or perl scripts, and the GROMACS analysis package tools.

Sequence alignment

Sequence alignment for the inverted topology analysis was performed using AlignME,[36] a program designed for pair-wise alignment of membrane protein sequences.

RESULTS

In this study, we performed extensive MD simulations and free energy calculations on three protein structures from two bacterial ASBT homologs. NmASBT was used as the prototype for substrate binding, as its X-ray structure contains two bound Na^+ and one bound TCH, and YfASBT was used as the prototype for the transport mechanism because its structures are suggested to consist of both outward-facing and inward-facing conformations (see Fig. 1).[20,21]

MD simulations of the three systems with and without bound Na^+ (up to two ions) and at the presence or absence of TCH were conducted for 100 ns each. In all the simulations, the transporter was stable (backbone atoms' RMSD of up to ~0.4 nm; see Supporting Information Fig. S3). The dynamics of the TCH molecule reveals stable binding, as it remained mostly bound throughout all the simulations to the same binding residues, suggesting that, kinetically, this duration is too short for TCH unbinding. Observing the behavior of the sodium ions revealed more insight, as described later.

Na^+ binding in NmASBT

To understand the transport cycle of ASBT, NmASBT was simulated with and without sodium ions bound to the binding sites revealed in the crystal structure. In the simulations where no Na^+ was initially present, no spontaneous Na^+ binding from the bulk occurred, probably because the simulation duration is not long enough for proper sampling that would result in binding. However, when Na^+ was present in the different sites, interesting observations were made. The Na^+ at Site I (see Fig. 1) was released to the intracellular bulk after ~20 ns as shown in Figure 2 left panel. In the simulation where TCH and both ions were bound, the Na^+ at Site I was released after 100 ns. Because this occurred near the end of the simulation, this particular simulation was extended by an additional 20 ns to ensure that the ion does not quickly rebind. Considering these two simulations, Site I binds Na^+ in a looser manner than Site II binds. To support this hypothesis, and refute the attribution of this to sporadic events, we computed free energy difference curves for Na^+ ions along the transporter.

PMF for NmASBT

Free energy difference curves for Na^+ binding along the transporter were calculated using umbrella sampling. As can be seen in Figure 3, Site I does not show an expected energy well characteristic of a binding site, with no observable trough. In contrast, an unexpected "cryptic" energy trough is seen along the coordinate, closer to the extracellular side. In the structure, this position corresponds to a zone adjacent to Site II, sharing residue Q264 (Q258 in YfASBT) that sterically could serve as a binding site (see Fig. 4 left panel). We hypothesize that this position, termed Site III, plays a key role in the transport cycle, serving as a putative third binding site that takes part in the translocation of the

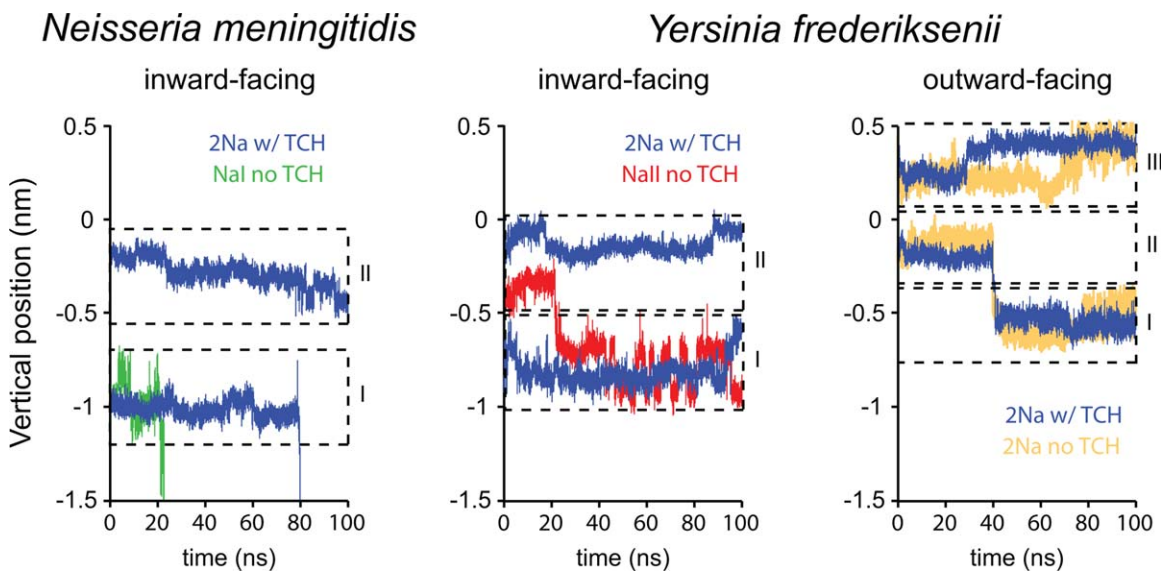

Figure 2

The position of the sodium ions along the *z*-axis is given as a function of time. The initial state of each simulation is indicated in colored text. NaI and NaII refer to Na^+ Site I and Site II binding, respectively; 2Na signifies that both ions were bound at the start of the simulation; w/ means "with." Binding site boundaries are marked with a dashed box. For visual clarity, in the NmASBT simulation in blue, the simulation time shown is 20–120 ns rather than 0–100 ns, respectively, as explained in the Results section. Only selected simulations are shown. [Color figure can be viewed in the online issue, which is available at wileyonlinelibrary.com.]

sodium ions, probably playing a more important part in conformations that have not yet been determined by structural means.

Site III consists of residues V105, G106, C108, and Q264 in the NmASBT sequence (corresponding to residues V99, G100, V102, and Q258 in the YfASBT sequence, respectively, see Fig. 4), positions that are highly conserved (data not shown). The interaction with the sodium ion is mediated by the backbone carbonyls of residues V105, G106, and C108, similarly to residues S128, E260, A261, and M263 in Sites I and II, and by the side chain of Q264.

Notably, in our SMD simulations, under the given applied conditions of force and speed, when the Na^+ was pulled in the direction of the extracellular side, its forced movement was substantially detained by interactions with nearby residues upon reaching the position of Site III. This is in line with the PMF curves, where we observe an energy trough, and supports the notion that an ion could structurally bind in that position. Furthermore, the energy barrier separating Site II from Site III is low enough to permit spontaneous translocation, presumably mediated by rotation of the side chain of Q264, which is shared by both Sites II and III.

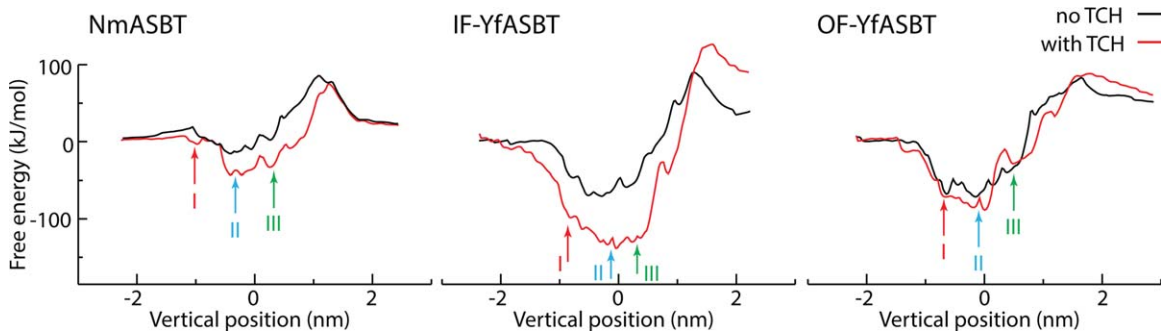

Figure 3

Free energy difference curves for Na^+ binding. The approximate position of Sites I, II, and III is marked with red, blue, and green arrows, respectively. The horizontal axis represents the *z*-coordinate in the simulation box, having negative values at the cytoplasmic side. At each panel, the red and black curves represent free energy calculations with and without TCH, respectively. [Color figure can be viewed in the online issue, which is available at wileyonlinelibrary.com.]

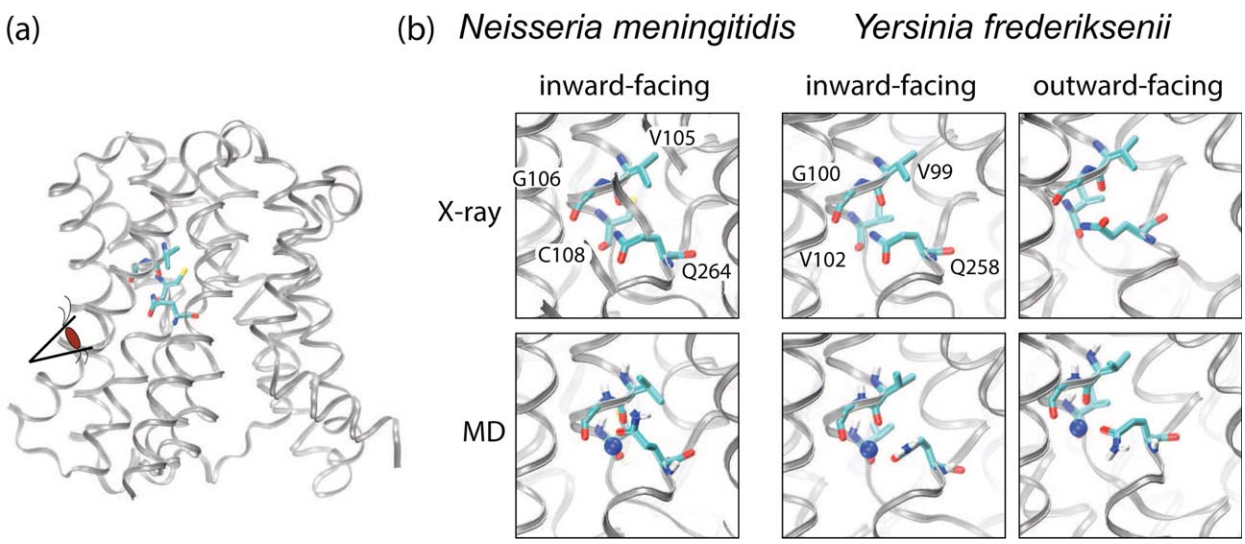

Figure 4

Atomic resolution visualization of binding Site III. (**a**) NmASBT in a ribbon representation; the residues of Site III are shown in a licorice representation. An eye shows the angle from which the snapshots in (b) are shown. (**b**) For each system, the X-ray structure (top) and a snapshot from a representative simulation (bottom) are shown. Na^+ is depicted in blue. [Color figure can be viewed in the online issue, which is available at wileyonlinelibrary.com.]

Free energy difference curves for the TCH molecule, moving from the cytoplasm to slightly above the binding site, were produced for the NmASBT as well. Four sets of simulations were run, to calculate the energetics of TCH binding in the absence of Na^+ and when ions were bound to Site I, II, or III (see Table I). The PMF curves for TCH revealed energetically favorable binding, as observed in the nonbiased simulations. The different curves were moderately similar, suggesting that Na^+ binding has little effect on the TCH binding (Fig. 5).

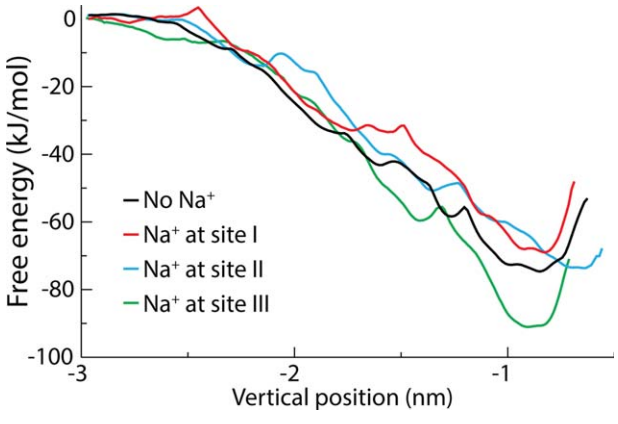

Figure 5

Free energy difference curves for TCH binding at the absence or presence of a bound Na^+ ion, as indicated. The horizontal axis represents the *z*-coordinate in the simulation box, having negative values at the cytoplasmic side. [Color figure can be viewed in the online issue, which is available at wileyonlinelibrary.com.]

Na^+ binding in YfASBT

The structure of the YfASBT has been determined in two conformations, inward-facing (IF) and a hypothesized outward-facing (OF) E254A mutant. The criteria supporting that the latter structure is indeed outward-facing are discussed in Ref. 21, and under the reasonable assumption that the wild-type transporter would assume the same conformation as the E254A mutant, we simulated the YfASBT in the two conformations.

In the simulations of the IF-YfASBT structure, we observed stability of the Na^+ bound to Site I (with or without bound TCH; data not shown), and when both sodium ions were bound; however, when the ion was bound to Site II, it moved to Site I (see Fig. 2 middle panel), which energetically seems to be less favorable (see Fig. 3).

In the OF-YfASBT simulations, we observe high stability of the Na^+ in the single ion simulations (data not shown); however, when two ions were bound to Sites II and III, the ion in Site II moved to Site I, probably due to electrostatic repulsion between the two bound Na^+ (see Fig. 2 right panel), a phenomenon observed at K^+ channels as well.[37,38] This is an interesting observation, because one might expect the ion at Site III to move toward the extracellular bulk, similar to the ion at Site I for the NmASBT simulations. This is further discussed later. Similarly to NmASBT, Site III interactions are mediated by the carbonyl oxygen atoms of V99, G100, and V102, as well as the side chain of Q258.

Finally, the bile acid molecule is stable in all the simulations of YfASBT. This suggests that the TCH molecule's

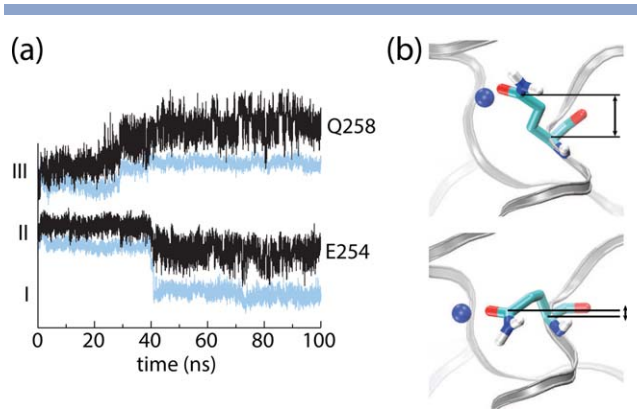

Figure 6

Residue orientation, OF-YfASBT with 2 Na^+ and TCH is shown as a representative simulation. (**a**) For each residue, the vertical distance between the side chain and the backbone atoms is shown in black. In shaded blue, at the background, are the sodium positions taken from Figure 2 right panel, blue. (**b**) Corresponding snapshots of Q258 from the simulation are shown for clarification of the distances presented. [Color figure can be viewed in the online issue, which is available at wileyonlinelibrary.com.]

k_{off} is too low to obtain unbinding during the simulation. Additionally, this supports the assumed binding site of the TCH in the OF conformation, suggested by Zhou *et al.*[21]

PMF for YfASBT

The PMF curves for the IF-YfASBT are qualitatively similar to the curves of the NmASBT structure; however, the energy magnitudes are higher in the YfASBT. In particular, the energy troughs for the IF-YfASBT at the presence of bile acid are very deep, and could be a consequence of sampling problems, compared with all other curves in Figure 3. Regardless, in both curves of the IF-YfASBT, the energy in Site I is higher than that in Site II and that in the hypothesized Site III.

The free energy difference curves of the OF-YfASBT, in contrast, seem to be somewhat of a mirror image of all other curves, where the energy for Site III is the highest. Based on the difference in the PMF curves, we simulated the structure of the OF-YfASBT with Na^+ bound at Sites II and/or III (see Table I). The reasoning behind this placement is in the core-domain's twofold pseudosymmetry[39]; the pair of occupied sites out of the three possible binding sites in the IF and OF conformations is expected to be different, as the energies are.

Residue orientation

An interesting observation was made while monitoring the orientation of certain residues, namely, residues Q77, N115, E260, and Q264 of NmASBT (corresponding to residues H71, N109, E254, and Q258, respectively, in the YfASBT sequence), all located in the vicinity of the binding sites. Throughout the simulations, when Na^+ ions were bound to the transporter, the polar side chain of the adjacent residue, from the list above, was constitutively facing the Na^+ ion (illustrated by the perfect synchronicity of a representative simulation shown in Fig. 6). Furthermore, when an ion was moving from one binding site to another, or unbinding a particular site, the adjacent residue rotated with the ion, "escorting" it along its trajectory.

Alignment

We performed sequence alignment of the two elements from the inverted repeat of NmASBT. The two inverted repeats were aligned to one another and are shown in Figure 7. The binding residues of Site II correspond to the binding residues of the hypothesized Site III (similar results were obtained for the YfASBT; data not shown).

DISCUSSION

Secondary active transporters couple the free energy stored in the electrochemical potential of one solute to the movement of another against its electrochemical potential. The mechanism of action of many secondary transporters follows the alternating access model, postulated by Jardetzky[40] and Mitchell.[41] According to the model, the transporter alternates between at least two conformational states in which the substrate- and the ion-binding sites are alternately exposed to the two sides of the membrane. From this structural mechanistic perspective, the crystal structures of ASBT were classified as inward-facing NmASBT,[20] inward-facing YfASBT,[21] and suggested as outward-facing structure YfASBT E254A mutant.[21] These structural data led to putative proposals of transport mechanisms of NmASBT and YfASBT.[20,21] Yet, the conformational states of NmASBT and YfASBT along the transport cycle are still obscure, and hence, we chose to address and track conformational dynamic features of ASBT transport by computational means.

Convergence of the free energy profiles

Free energy profiles are an instrumental part of this study, and hence, assessing their convergence is of high importance. To that end, at all the PMF simulations, we verified convergence by using a subsampling of the entire production run, and re-performed the calculations using only the first half of each production run (Supporting Information Fig. S4). The subsampling free energy curves are quantitatively very similar to the curves with the entire length duration production run, demonstrating that the curves shown on Figures 3 and 5 have adequately converged (see Supporting Information). Notably, convergence of free energy profiles of PMF calculations was addressed and evaluated by other

Figure 7

Sequence alignment of the two inverted repeats of NmASBT. Residues of Sites I, II, and III are marked in red, blue, and green, respectively. Residues shared by two binding sites are highlighted in the two respective colors. The alignment was performed following Ref. 36; however, a gap that was suggested by the program has been omitted to account for helix alignment on the solved structure. TM helices are marked by an underline. [Color figure can be viewed in the online issue, which is available at wileyonlinelibrary.com.]

methodological approaches as well. For example, solving the WHAM equations by maximizing a target likelihood function by developing optimization algorithms with a faster convergence rate than the common procedure,[42] using two different sets of starting structures, one from unbiased and the other from biased MD simulations,[43] increasing the sampling time for each window,[44,45] and generating multiple sets of simulations from different starting conformations.[45]

A putative binding site for Na^+

We conducted extensive simulations and free energy calculations on the three available published structures. Our free energy difference curves suggest the existence of a third sodium ion binding site that is not occupied in any of the X-ray structures. This is based on the appearance of a distinct energy well in each of the free energy difference curves (Fig. 3), as well as in SMD simulations where pulling of the ion through the position termed Site III resulted in trapping of the ion. The existence of Site III is also hinted in the sequence, where the binding residues of Site III correspond to the binding site of the assumed inverted topology of ASBT (Fig. 7).

In the determined crystallographic structure of YfASBT, there was no obvious electron density for Na^+ at Site I and a very weak density at Site II. Consequently, the determined positions of the Na^+ ions at the crystal structure are only an estimation.[21] Thus, because electron density was not seen at the putative location of Site III, its existence was not proposed or even checked experimentally. We suggest that Site III has a functional role as a binding site in several conformations, providing energetically favorable access for the Na^+ to the outside of the cell. Altogether, the binding sites are separated by relatively low energy barriers, enabling movement of the Na^+ ion from site to site with relative ease, according to the current conformational state.

Although the existence of the third binding site is speculative, and no experimental evidence has confirmed it to date, the presence of unseen binding sites in crystallographic structures was previously suggested by other independent studies, and such binding sites have been revealed in various different systems. For example, a third Na^+ binding site in GltPh,[46,47] a fourth one for the Na^+,K^+-ATPase,[48] a third one for BetP,[49] an additional secondary binding site in LeuT,[50–52] and an additional binding site for K^+ in KcsA.[53] Thus, in a membrane transport protein, the presence of an additional binding site for an ion that is not observed in the crystal structure (probably due to unclear or absence of electron density) may be plausible and even advantageous because it can contribute to binding and stepwise shuttling of the ions.

Chemically speaking, it should be mentioned that the ideal coordination number for sodium ions is six, as observed in the crystal structure for ions bound to Sites I and II of the NmASBT.[20] According to our results, the coordination number for the sodium ion in Site III is four, in most of the simulation time, namely the carbonyl oxygens of V105, G106, and C108 as well as the side chain group of Q264 (corresponding to V99, G100, V102, and Q258, respectively; see Fig. 4). These findings do not contradict our hypothesis because it was found that the bacterial melibiose permease (MelB) is characterized by coordination of four[54,55] crystal structures of the bacterial homologue of LeuT[56] and the sodium/galactose symprorter (vSGLT)[57] show coordination number of five at the Na^+ binding site, and the Na^+ binding sites at BetP show different coordination numbers that varies at the conformational states of the protein.[49]

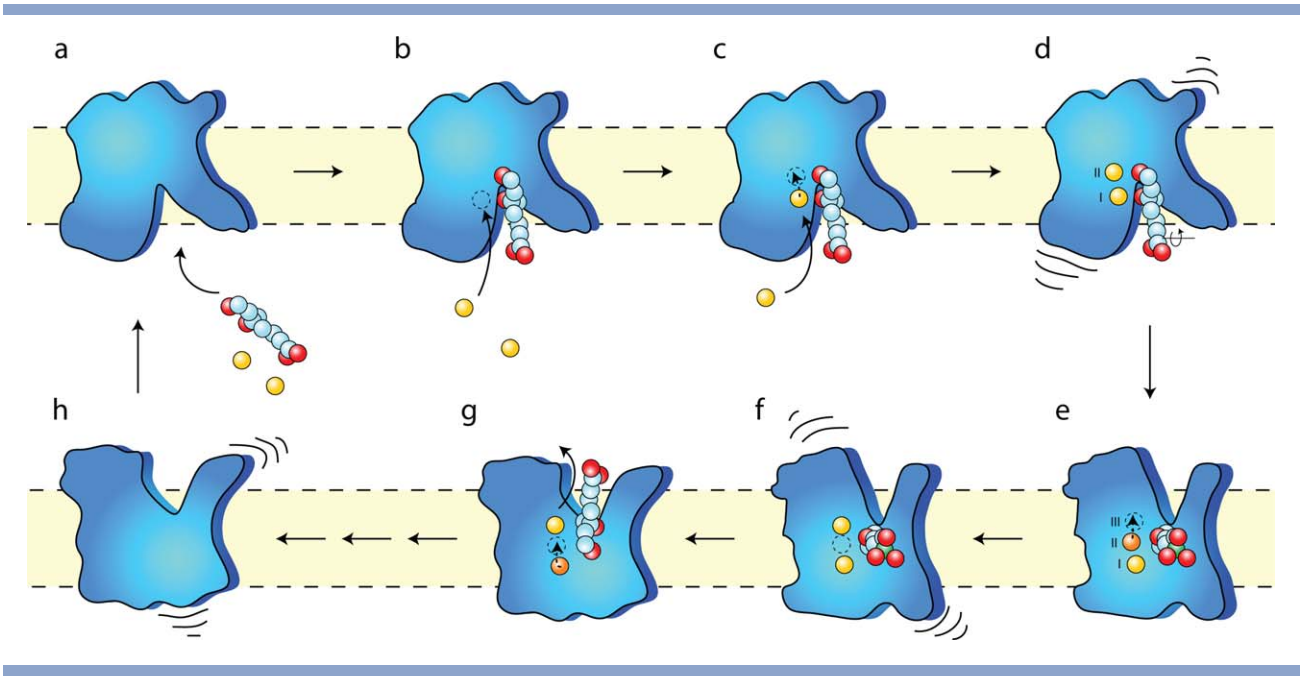

Figure 8

Transport cycle illustration for the bacterial ASBT as detailed in the Discussion section. The cytoplasm is below each membrane bilayer, depicted as a pale yellow strip. Sodium ions are depicted in yellow, having orange coloring describing a repulsive force. The TCH molecule is depicted in cyan and red spheres. Conformational changes are marked as line triplets. The positions of empty binding sites are depicted for clarity as dashed circles in several steps, however present in all conformations. The binding site numbers are shown in steps (**d**) and (**e**) and apply for all conformations. The process is fully reversible, but unidirectional arrows are used for visual clarity.

The orientation of several residues in the core domain

We propose that the flexibility and dynamics of several key residues in the core domain is functionally significant; namely, residues Q77, N115, E260, and Q264 of NmASBT (corresponding to residues H71, N109, E254, and Q258 in the YfASBT sequence). All these residues are highly conserved (data not shown), and mutations of Q77 and E260 in NmASBT and of E254 and Q258 in YfASBT markedly affect activity.[20,21] These residues are located at the interfaces of the bulk and the binding sites, and careful examination of their rotamer orientation in the simulations reveals that they are facing toward the bound sodium ions (see Fig. 6). We hypothesize that these residues serve as molecular arms, mediating the movement of sodium ions from one site to the other (e.g., Q264; see shared residues in Fig. 7), or from Site I to the intracellular bulk (N115). Residues with a similar role have been reported for other transporters, such as NorM.[58]

Mechanism of action

To gain more understanding on the ASBT structural features, it is advised to put the above conclusions into mechanistic perspective. Hence, we integrate and incorporate our results into a putative transport cycle that obeys to the alternative access mechanism. Studies using patch clamped transfected cells demonstrated that human ASBT can mediate bidirectional bile acid transport, and the directionality was determined by the sodium gradient and membrane potential.[15] It is reasonable to assume that the same holds true for the bacterial ASBT, and therefore, the transport cycle should be bidirectional as well. Using the information obtained from the simulations, it seems more intuitive to suggest a reversible cycle of transport where the TCH molecule and sodium ions are being pumped from the inside to the outside of the cell.

Based on the PMF curves, it would seem that the stability of the ion in Site I is particularly low in the absence of the bile acid molecule (Fig. 3). Therefore, we suggest that the first element to bind would be the bile acid molecule [Fig. 8(a)]. Another possibility is simultaneous binding, as recently reported for the H^+/Cl^- exchanger.[59] Next, a sodium ion should bind, probably at binding Site I, which is accessible to the bulk [Fig. 8(b)]. Subsequently, as a second ion nears the binding site, the ions would slide into positions I and II in a concerted and coordinated manner, for the second and first ions, respectively [Fig. 8(c)]. This "knock-on" mechanism has been observed and suggested to be a hallmark of Na^+ binding sites in transporters,[60] where the presence of a second ion at its own binding site induces the movement of the first ion from its binding site.

These two steps depict the reverse of the process that occurred in the simulations shown in Figure 2 for the NmASBT and the IF-YfASBT, in line with the bidirectional nature of the transport cycle. At this point, the transporter exists in the state that appears in the crystal structure of the NmASBT [Fig. 8(d)]. The PMF curves suggest that the next step is movement of the sodium ions from Sites I and II to Sites II and III, which may set up a series of events that lead to a conformational transition from the inward- to the outward-facing conformation. This structural change [the transition to Fig. 8(e)] has been discussed extensively by Zhou *et al.*[21] In the outward-facing state, the simulations suggest that Sites II and III cannot be occupied simultaneously (see Fig. 2); yet, it seems unlikely that ions would move from Sites I or II directly to the extracellular bulk, as no water is accessible to these sites from the extracellular side. We suggest that the ions are released from Site III, and that the outward-facing state of the YfASBT structure represents an intermediate conformation. In this intermediate conformation, our simulations suggest that the ions are bound to Sites I and III [Figs. 2 and 8(f)]. Hence, we propose another conformational state, similar to the outward-facing conformation presented, in which Site I is completely occluded and cannot bind, forcing the ions to bind to Sites II and III, noting that occluded states are a common feature of transport cycles. This in turn, will produce an electrostatic repulsion that would result in the ion bound to Site III to leave into the bulk [Fig. 8(g)]. The next steps would be release of the second sodium ion and of the bile acid; the order cannot be inferred from the data we have; however, symmetry considerations would favor unbinding of the sodium prior to the unbinding of the bile acid molecule. The last step is a conformational change of the outward-facing apo ASBT back to the inward-facing conformation, to reset and proceed to the next transport cycle [Fig. 8(h)]. The complete suggested cycle is shown in Figure 8.

Concluding remarks

To summarize, we propose, based on computational simulations and calculations, the existence of a third binding site that is involved in the transport cycle of ASBT. We suggest a detailed mechanism of action for ASBT, involving eight distinct sequential states, in three conformations [represented by Fig. 8(a,e,g)]; two of them are based on the existing crystal structures. We emphasize that this proposed transport mechanism may be provisional and incomplete, and future experiments are required for its verification, and most probably for specific modifications. Yet, we believe that it postulates the crucial conformational states of ASBT that are present along the transport cycle. Thus, although speculative, we hope that our work will encourage experimental studies to confirm our hypothesis as well as promote understanding on the transport cycle of ASBT and transport mechanism altogether.

ACKNOWLEDGMENTS

I.T.A. is the Arthur Lejwa Professor of Structural Biochemistry at the Hebrew University of Jerusalem.

REFERENCES

1. Hofmann AF, Hagey LR. Bile acids: chemistry, pathochemistry, biology, pathobiology, and therapeutics. Cell Mol Life Sci 2008;65:2461–2483.
2. Dawson PA, Lan T, Rao A. Bile acid transporters. J Lipid Res 2009; 50:2340–2357.
3. Claro da Silva T, Polli JE, Swaan PW. The solute carrier family 10 (SLC10): beyond bile acid transport. Mol Aspects Med 2013;34:252–269.
4. Döring B, Lütteke T, Geyer J, Petzinger E. The SLC10 carrier family: transport functions and molecular structure. Curr Top Membr 2012;70:105–168.
5. Bhat BG, Rapp SR, Beaudry JA, Napawan N, Butteiger DN, Hall KA, Null CL, Luo Y, Keller BT. Inhibition of ileal bile acid transport and reduced atherosclerosis in apoE-/- mice by SC-435. J Lipid Res 2003;44:1614–1621.
6. Braun A, Yesilaltay A, Acton S, Broschat KO, Krul ES, Napawan N, Stagliano N, Krieger M. Inhibition of intestinal absorption of cholesterol by ezetimibe or bile acids by SC-435 alters lipoprotein metabolism and extends the lifespan of SR-BI/apoE double knockout mice. Atherosclerosis 2008;198:77–84.
7. Wu Y, Aquino CJ, Cowan DJ, Anderson DL, Ambroso JL, Bishop MJ, Boros EE, Chen L, Cunningham A, Dobbins RL, Feldman PL, Harston LT, Kaldor IW, Klein R, Liang X, McIntyre MS, Merrill CL, Patterson KM, Prescott JS, Ray JS, Roller SG, Yao X, Young A, Yuen J, Collins JL. Discovery of a highly potent, nonabsorbable apical sodium-dependent bile acid transporter inhibitor (GSK2330672) for treatment of type 2 diabetes. J Med Chem 2013;56:5094–5114.
8. Jahnel J, Fickert P, Hauer AC, Högenauer C, Avian A, Trauner M. Inflammatory bowel disease alters intestinal bile acid transporter expression. Drug Metab Dispos 2014;42:1423–1431.
9. Bergheim I, Harsch S, Mueller O, Schimmel S, Fritz P, Stange EF. Apical sodium bile acid transporter and ileal lipid binding protein in gallstone carriers. J Lipid Res 2006;47:42–50.
10. Walters JR. Defining primary bile acid diarrhea: making the diagnosis and recognizing the disorder. Expert Rev Gastroenterol Hepatol 2010;4:561–567.
11. Nagengast FM, Grubben MJ, van Munster IP. Role of bile acids in colorectal carcinogenesis. Eur J Cancer 1995;31A:1067–1070.
12. Ou J, DeLany JP, Zhang M, Sharma S, O'Keefe SJ. Association between low colonic short-chain fatty acids and high bile acids in high colon cancer risk populations. Nutr Cancer 2012;64:34–40.
13. Zheng X, Ekins S, Raufman JP, Polli JE. Computational models for drug inhibition of the human apical sodium-dependent bile acid transporter. Mol Pharm 2009;6:1591–1603.
14. Ajouz H, Mukherji D, Shamseddine A. Secondary bile acids: an underrecognized cause of colon cancer. World J Surg Oncol 2014;24:164.
15. Weinman SA, Carruth MW, Dawson PA. Bile acid uptake via the human apical sodium-bile acid cotransporter is electrogenic. J Biol Chem 1998;273:34691–34695.
16. Moore RH, Chothe P, Swaan PW. Transmembrane domain V plays a stabilizing role in the function of human bile acid transporter SLC10A2. Biochemistry 2013;52:5117–5124.
17. Khantwal CM, Swaan PW. Cytosolic half of transmembrane domain IV of the human bile acid transporter hASBT (SLC10A2) forms part of the substrate translocation pathway. Biochemistry 2008;47: 3606–3614.

18. Oelkers P, Kirby LC, Heubi JE, Dawson PA. Primary bile acid malabsorption caused by mutations in the ileal sodium-dependent bile acid transporter gene (SLC10A2). J Clin Invest 1997;99: 1880–1887.
19. Ho RH, Leake BF, Urquhart BL, Gregor JC, Dawson PA, Kim RB. Functional characterization of genetic variants in the apical sodium-dependent bile acid transporter (ASBT; SLC10A2). J Gastroenterol Hepatol 2011;26:1740–1748.
20. Hu NJ, Iwata S, Cameron AD, Drew D. Crystal structure of a bacterial homologue of the bile acid sodium symporter ASBT. Nature 2011;478:408–411.
21. Zhou X, Levin EJ, Pan Y, McCoy JG, Sharma R, Kloss B, Bruni R, Quick M, Zhou M. Structural basis of the alternating-access mechanism in a bile acid transporter. Nature 2014;505:569–573.
22. Screpanti E, Hunte C. Discontinuous membrane helices in transport proteins and their correlation with function. J Struct Biol 2007;159: 261–267.
23. Hunte C, Screpanti E, Venturi M, Rimon A, Padan E, Michel H. Structure of a Na^+/H^+ antiporter and insights into mechanism of action and regulation by pH. Nature 2005;435:1197–1202.
24. Tieleman DP, Berendsen HJ. A molecular dynamics study of the pores formed by *Escherichia coli* OmpF porin in a fully hydrated palmitoyloleoylphosphatidylcholine bilayer. Biophys J 1998;74:2786–2801.
25. Van Der Spoel D, Lindahl E, Hess B, Groenhof G, Mark AE, Berendsen HJC. GROMACS: fast, flexible, and free. J Comput Chem 2005;26:1701–1718.
26. Berendsen H, van der Spoel D, van Drunen R. GROMACS: a message-passing parallel molecular-dynamics implementation. Comput Phys Commun 1995;91:43–56.
27. Siu SWI, Vácha R, Jungwirth P, Böckmann RA. Biomolecular simulations of membranes: physical properties from different force fields. J Chem Phys 2008;128:125103.
28. Hess B, Bekker H, Berendsen H, Fraaije J. LINCS: a linear constraint solver for molecular simulations. J Comput Chem 1997;18:1463–1472.
29. Darden T, York D, Pedersen L. Particle mesh Ewald: an N-log(N) method for Ewald sums in large systems. J Chem Phys 1993;98: 10089–10092.
30. Koziara KB, Stroet M, Malde AK, Mark AE. Testing and validation of the Automated Topology Builder (ATB) version 2.0: prediction of hydration free enthalpies. J Comput Aided Mol Des 2014;28:221–233.
31. Schneidman-Duhovny D, Inbar Y, Nussinov R, Wolfson HJ. PatchDock and SymmDock: servers for rigid and symmetric docking. Nucleic Acids Res 2005;33(Web Server issue):W363–W367.
32. Israelewitz B, Baudry J, Gullingsrud J, Kosztin D, Schulten K. Steered molecular dynamics investigations of protein function. J Mol Graph Model 2001;19:13–25.
33. Dickson A, Dinner AR. Enhanced sampling of nonequilibrium steady states. Annu Rev Phys Chem 2010;61:441–459.
34. Kumar S, Bouzida D, Swendsen R, Kollman P, Rosenberg J. The weighted histogram analysis method for free-energy calculations on biomolecules. 1. The method. J Comput Chem 1992;13:1011–1021.
35. Humphrey W, Dalke A, Schulten K. VMD: visual molecular dynamics. J Mol Graph 1996;14:33–38.
36. Stamm M, Staritzbichler R, Khafizov K, Forrest LR. Alignment of helical membrane protein sequences using AlignMe. PLoS One 2013;8:e57731.
37. Hodgkin AL, Keynes RD. The potassium permeability of a giant nerve fibre. J Physiol 1955;128:61–88.
38. Bernèche S, Roux B. Energetics of ion conduction through the K^+ channel. Nature 2001;414:73–77.
39. Radestock S, Forrest LR. The alternating-access mechanism of MFS transporters arises from inverted-topology repeats. J Mol Biol 2011; 407:698–715.
40. Jardetzky O. Simple allosteric model for membrane pumps. Nature 1966;211:969–970.
41. Mitchell P. A general theory of membrane transport from studies of bacteria. Nature 1957;180:134–136.
42. Zhu F, Hummer G. Convergence and error estimation in free energy calculations using the weighted histogram analysis method. J Comput Chem 2012;33:453–465.
43. Paloncýová M, Berka K, Otyepka M. Convergence of free energy profile of coumarin in lipid bilayer. J Chem Theory Comput 2012;8: 1200–1211.
44. Gkeka P, Angelikopoulos P, Sarkisov L, Cournia Z. Membrane partitioning of anionic, ligand-coated nanoparticles is accompanied by ligand snorkeling, local disordering, and cholesterol depletion. PLoS Comput Biol 2014;10:e1003917.
45. Neale C, Drew Bennett WF, Tieleman DP, Pomès R. Statistical convergence of equilibrium properties in simulations of molecular solutes embedded in lipid bilayers. J Chem Theory Comput 2011;7: 4175–4188.
46. Bastug T, Heinzelmann G, Kuyucak S, Salim M, Vandenberg RJ, Ryan RM. Position of the third Na^+ site in the aspartate transporter GltPh and the human glutamate transporter, EAAT1. PLoS One 2012;7:e33058.
47. Huang Z, Tajkhorshid E. Identification of the third Na^+ site and the sequence of extracellular binding events in the glutamate transporter. Biophys J 2010;99:1416–1425.
48. Nyblom M, Poulsen H, Gourdon P, Reinhard L, Andersson M, Lindahl E, Fedosova N, Nissen P. Crystal structure of Na^+, K^+-ATPase in the Na^+-bound state. Science 2013;342:123–127.
49. Perez C, Faust B, Mehdipour AR, Francesconi KA, Forrest LR, Ziegler C. Substrate-bound outward-open state of the betaine transporter BetP provides insights into Na^+ coupling. Nat Commun 2014;5:4231.
50. Shi L, Quick M, Zhao Y, Weinstein H, Javitch JA. The mechanism of a neurotransmitter:sodium symporter-inward release of Na^+ and substrate is triggered by substrate in a second binding site. Mol Cell 2008;30:667–677.
51. Celik L, Schiøtt B, Tajkhorshid E. Substrate binding and formation of an occluded state in the leucine transporter. Biophys J 2008;94: 1600–1612.
52. Zomot E, Gur M, Bahar I. Microseconds simulations reveal a new sodium-binding site and the mechanism of sodium-coupled substrate uptake by LeuT. J Biol Chem 2015;290:544–555.
53. Roux B, MacKinnon R. The cavity and pore helices in the KcsA K^+ channel: electrostatic stabilization of monovalent cations. Science 1999;285:100–102.
54. Ethayathulla AS, Yousef MS, Amin A, Leblanc G, Kaback HR, Guan L. Structure-based mechanism for Na^+/melibiose symport by MelB. Nat Commun 2014;5:3009.
55. Granell M, León X, Leblanc G, Padrós E, Lórenz-Fonfría VA. Structural insights into the activation mechanism of melibiose permease by sodium binding. Proc Natl Acad Sci U S A 2010;107:22078–22083.
56. Yamashita A, Singh SK, Kawate T, Jin Y, Gouaux E. Crystal structure of a bacterial homologue of Na^+/Cl^--dependent neurotransmitter transporters. Nature 2005;437:215–223.
57. Faham S, Watanabe A, Besserer GM, Cascio D, Specht A, Hirayama BA, Wright EM, Abramson J. The crystal structure of a sodium galactose transporter reveals mechanistic insights into Na^+/sugar symport. Science 2008;321:810–814.
58. Leung YM, Holdbrook DA, Piggot TJ, Khalid S. The NorM MATE transporter from *N. gonorrhoeae*: insights into drug and ion binding from atomistic molecular dynamics simulations. Biophys J 2014;107: 460–468.
59. Picollo A, Xu Y, Johner N, Bernèche S, Accardi A. Synergistic substrate binding determines the stoichiometry of transport of a prokaryotic H^+/Cl^- exchanger. Nat Struct Mol Biol 2012;19: 525−531, S1.
60. Zdravkovic I, Zhao C, Lev B, Cuervo JE, Noskov SY. Atomistic models of ion and solute transport by the sodium-dependent secondary active transporters. Biochim Biophys Acta 2012;1818: 337–347.